ISSN 2303-8403 Broj 2, 2016

ESTIMATE OF INDUCED SEISMICITY PARAMETERS OF GEOMECHANICAL OBJECTS BASED ON MATHEMATICAL MODELING USING LABORATORY TEST DATA AND FIELD OBSERVATION

Larisa Nazarova
Geomechanics, Institute of Mining, Siberian Branch of the Russian Academy of Science, Krasny Prospekt 54, Novosibirsk, Russia, 630091
Leonid Nazarov
Geomechanics, Institute of Mining, Siberian Branch of the Russian Academy of Science, Krasny Prospekt 54, Novosibirsk, Russia, 630091

Summary:

Joint analysis of micro-displacements recorded by white light speckle-photography method on the surface of diametrically compressed disc-shaped rock sample and simulated elastic macro-stress field was carried out. The probably significant relationships between the damage in the different parts of a sample as well as the level of the external load were uncovered. In crucial respect, having a verified model of geomechanical object describing stress field evolution it affords base for estimation the damage rate of the object by monitoring of state of it single part.

The developed approach applied for analysis of the space-time correlation relationships between parameters of induced seismicity (number of seismic events, stochastic data) and the stress state variation (deterministic information) in coarse of mining of Tashtagol iron-ore deposit.

Keywords:

rock mass, stress field, mining, induced seismicity, laboratory experiment, white light speckle photography, 3D geomechanical model, Tashtagol iron-ore deposit

1. INTRODUCTION

High-technology mines and collieries are equipped with Mining Monitoring and Control Systems (MCS) for recording and processing of seismic information (microseismic emission, MSE) in geomechanical space of underground objects [1,2]. Most of MCS carry out passive monitoring [3] and data are interpreted by statistical methods based on the damage accumulation criterion [4] or using seismologic approach [5]. The modern tendency of mining geophysics consists in development of methods to reveal space-time relations between parameters of MSE and the stress-strain state of a rock mass. The empirical dependencies of even count, acoustic emission count rate on axial stress and confining pressure applied to rock sample were elicited in laboratory experiments without localization of acoustic events sources [6,7]. The shots were taken to find relations between parameters of simulated stress field and seismicity level using synthetic [8] and *in situ* [9] data in order to predict dynamic phenomena in a rock mass.

The aims of the present article are: to substantiate an approach to interpretation of random data in order to establish the quantitative relations between damage of different parts of test rock sample under loading; to apply the approach to investigation of seismicity induced by stress field evolution at operating mine.

2. EXPERIMENTAL INVESTIGATION OF DAMAGE EVOLUTION IN ROCK SAMPLES

2.1. Equipping and experimental design

Brazilian tests were carried out on cylinder-shaped marble samples (10 mm in thickness, radius $r_S = 15$ mm, Young modulus $E = 37$ GPa, Poisson ratio $\nu = 0.11$). At the lateral surface of the cylinder parallel bevels of $l = 5$ mm in length were milled to assure the contact with plates of the loading device (Chart 1). Vertical overhauling load was applied with measurement of pressure P in the hydraulic system of device. Simultaneously, speckle-photos were taken (White Light Speckle Photography technique – WLSP [10]) in zone R (height $X = 29$ mm, length $Y = 10$ mm) at the front base of the cylinder to record microdisplacements $u_x(x,y,m)$, $u_y(x,y,m)$, m is stage of loading ($m=1,\ldots,M$), (x,y) are Cartesian coordinates (Chart 1*c*). Using u_x and u_y we calculate the microstrains $e_{ij}(x,y,m)$ $(i, j=x, y)$ by triangulation of R.

Resolution of WLSP apparatus Almec-TV is 65×25 points, recording was carried out for $0 \le P(m) \le P_t$, where P_t - pressure at which calculated tensile strength σ_t [11] appeared equal to 12 MPa, $P(m) = mP_t / M$. The total number of frames was $M = 400$.

Chart 1. Experimental plant (a, b): 1 – yoke of loading device (Instron 8802); 2 – WLSP system Almec-TV; 3 – plates; 4 – rock sample; R – illumination zone of Almec-TV, where microdisplacements are recorded; (c) simulation model.

2.2. Elastic stress-strain state in circular domain under diametric compression

Solution of the elastic problem on the stress state of a circular domain under diametric compression at $\alpha \neq 0$ was first obtained in the 1950s in the form of infinite series [12]. It appeared that these series were summable and we found analytical expressions of stress field components in cylindrical coordinate system (r,θ):

$$\begin{aligned} \sigma_{rr} &= P(\alpha - S_1 + S_2)/\pi \\ \sigma_{\theta\theta} &= P(\alpha + S_1 + S_2)/\pi \\ \sigma_{r\theta} &= 2P(\xi^2-1)(1-\xi^4)\cos 2\theta \sin\alpha/(\pi D_- D_+) \end{aligned} \qquad (1)$$

where $\xi = r/r_S$, $D_\pm = 1 - 2\xi^2\cos(2\theta \pm \alpha) + \xi^4$, $S_1 = 2(\xi^2-1)[(1+\xi^4)\cos 2\theta - 2\xi^2\cos\alpha]/(D_- D_+)$, $S_2 = \arctan G_+ - \arctan G_-$, $G_\pm = \xi^2 \sin(2\theta \pm \alpha)/[1 - 2\xi^2\cos(2\theta \pm \alpha)]$.

Chart 2a demonstrates level lines of the maximal shear stress τ_{max}/P calculated by (1). For comparison Chart 2b presents the distribution of τ_{max}, obtained by the photoelastic method [13]. The quantitative match of the images is clearly obvious when the second distribution is be multiplied by the appropriate conversion factor.

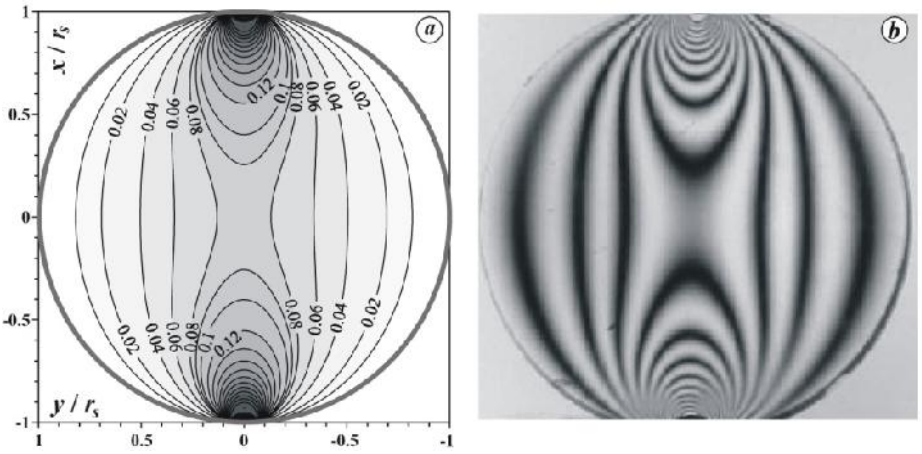

Chart 2. Distribution of maximum shear stress τ_{max} : analytical solution (a); photoelastic method after [13] (b).

2.3. Damage distribution in a sample under loading according to speckle photography data

Processing of acoustic emission data under loading of rock sample is built upon association of every impulse with the origin of a new flaw or propagation of existing one [6,7]. Hence, criteria of strength and/or crack growth are disregarded, as it is impossible to take into account the scale effect at the microstructure level.

We suggest the following criterion: a new flaw arises at a given point (x,y) if

$$e_1(x,y,m) = e_* , \qquad (2)$$

where e_1 is the extensional principal strain calculated by WLSP data e_{ij}, the empirical limit e_* of the extension strength for each sample was chosen so that at $P = 0.8P_t$ equality (2) is valid in the central part of line $Y=0$ (Chart 1). Domain R was divided into equal subdomains R_k $(k = 2,\ldots,K)$, wherein number $N_k(m)$ of points to meet condition (2) was counted at every loading stage m.

Chart 3*a-c* presents flaws locations in the domain R at $P(m) = 0.15P_t$, $0.3P_t$, $0.45P_t$ $(m = 60,\ 120,\ 180)$ qualitatively corresponding to distribution of the first principal macrostrain ε_1 (Chart 3*d*, positive values – elongation) calculated by Hooke's law and stresses (1).

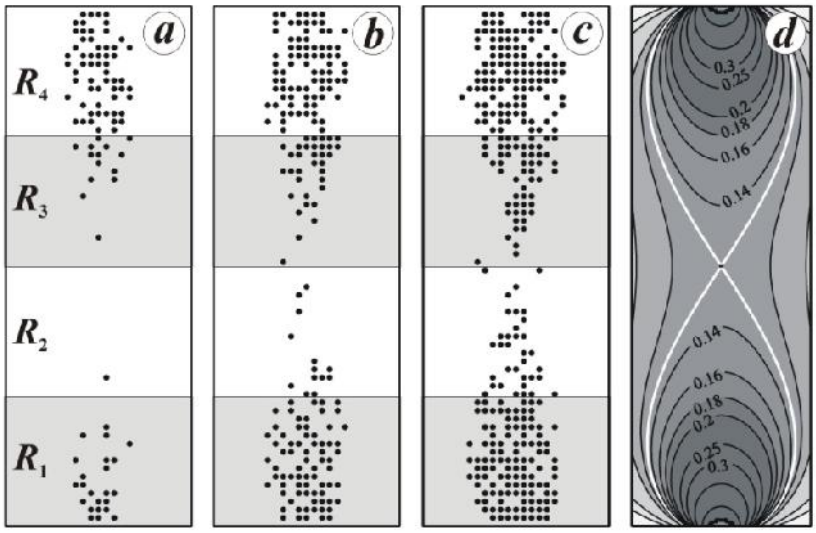

Chart 3. Location of flaw in domain R at different loading stages (a,b,c); distribution of the strain £N reduced to E\P (d).

2.4. Correlation analysis of damage

Chart 4*a*,*b* demonstrates dependencies of N_k on m at division of R into three and four parts. It is seen that in the middle parts of R the stable increase in N_k starts under the external load greater than approximately $P_c \cong 0.35P_t$.($m_c \cong 140$).

Calculate the cross-correlation indices c_{ik} ($i = 2,\ldots,K$) between number of flaws in subdomains of R:

$$c_{ik}(N_i(m), N_k(m)) = \frac{\sum_{n=0}^{m} Q_{in}Q_{kn}}{\pm(N_i(m))\pm(N_k(m))}, \qquad \pm^2(N_i(m)) = \sum_{n=0}^{m} Q_{in}^2,$$

where $Q_{ik} = N_k(n) - A_k$, A_k is an average value of N_k at $0 \le n \le m$. They describe the quantitative relation between damage degree in different parts of sample. It is important to keep in mind that at $P > P_c$ indices c_{ik} are higher than 0.8.

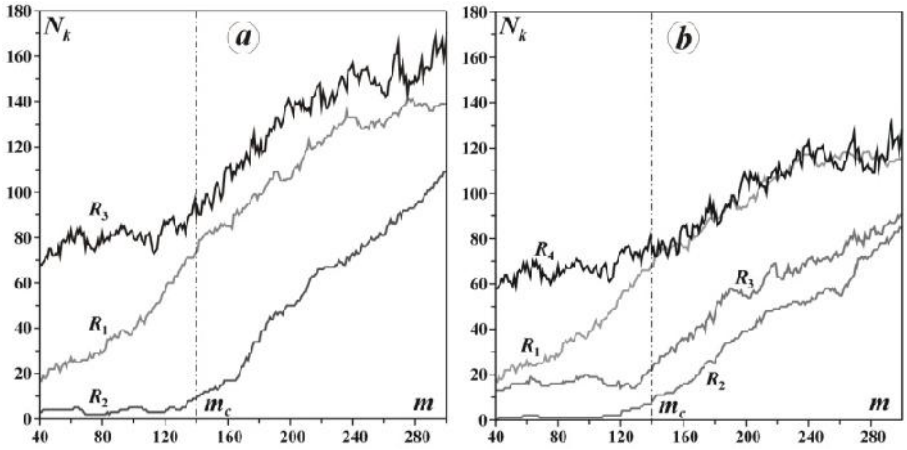

Chart 4. Number of flaws N_k in subdomain R_k via load level m at different K: a – KZP; b - KZQ.

ISSN 2303-8403 Broj 2, 2016

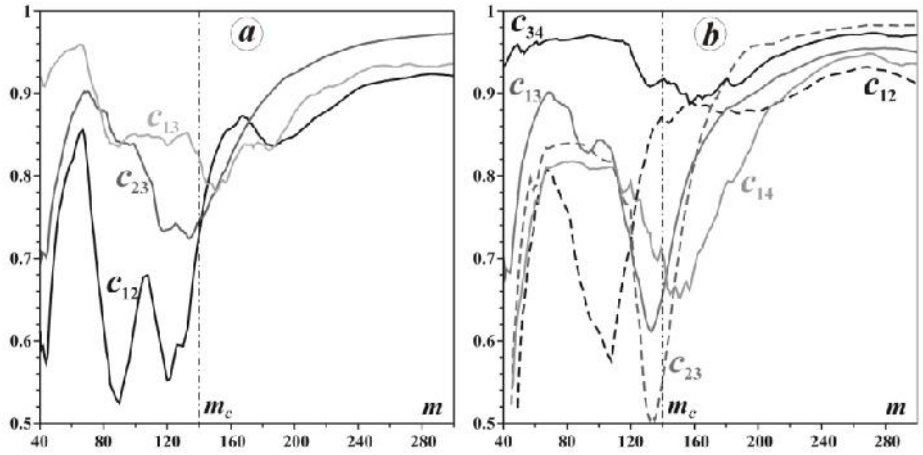

Chart 5. Cross-correlation indices c_{ik} via load level m at different K: a – KZP; b - KZQ.

Under domain *R* partitioning into other number of equal parts the revealed quantitative relations remain the same with negligible variations in c_{ik}. This proves the possibility to evaluate a damage level in the entire domain under investigation by controlling the state of some subdomain only.

3. STRESS FIELD EVOLUTION AND INDUCED SEISMICITY IN TASHTAGOL IRON-ORE MINE

Mining operations at deeper levels and the expansion of mining have resulted in greater load on rock masses and stress redistribution, thus inducing dangerous dynamic events (rock bursts, induced quakes) and other rock pressure events in mines and its geomechanical space [14,15]. The study object of the modern quantitative seismology is the *a posteriori* analysis of seismograms aimed to evaluate focal parameters of earthquakes and to find statistically the space-time regularities of a seismic process, neglecting variations in stress fields within a geological medium subjected to geodynamic influence [16].

Let us apply the above-developed approach to find the space-time relations between the number of seismic events and the stress state parameters through the correlation analysis of random data on induced seismicity and nonprobabilistic data on variation of geomechanical fields.

3.1. Geological structure and geomechanical model of object under investigation

Tashtagol iron-ore deposit (Altay-Sayan folded belt) consists of superimposed lens-shaped sub-vertical ore bodies. The ore zone ranges from 10 to 100 m in thickness and is up to 600 m in extension. The ore bodies are intersected by microsyenite porphyry and diabase dykes, from few centimeters up to 10 m in thickness, and faults 5-30 m thick. At the present time the depth of mining is about 900 m (Level – 350 m).

The volume geomechanical model of the Tashtagol deposit has been developed in [17], taking into account high horizontal components σ_h and σ_H of natural stress field, surface topography, basic faults and variations in mined-out space configuration (Chart 6). Anticipatory appraisal of σ_h, σ_H by seismotectonical data [18] has shown that $\sigma_h = 1.3\sigma_V$, $\sigma_H = 2.5\sigma_V$ (σ_V - lithostatic pressure). The proprietory finite element code developed in [17,19] was used for model implementation.

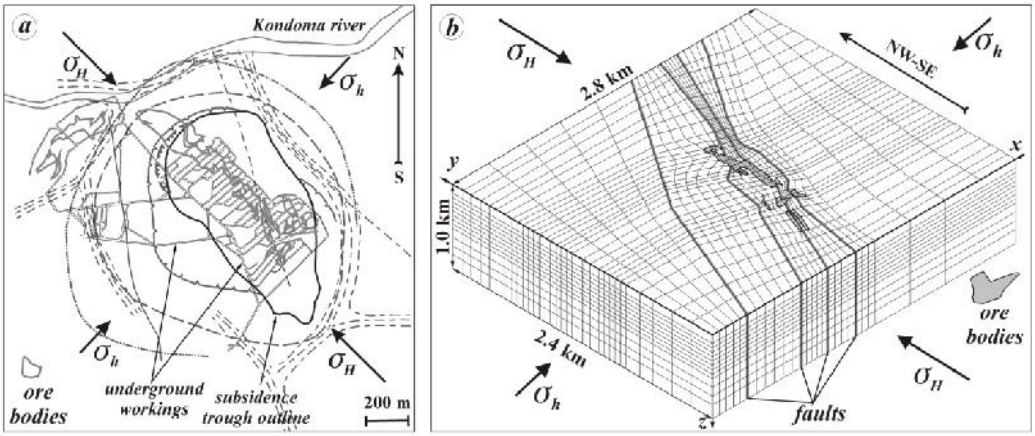

Chart 6. Scheme of Tashtagol deposit (a); geometrical model and FEM mesh associated with fault structure (b).

Level lines of the maximum shear stress τ_{max} in consecutive steps of deposit exploitation are exemplified in Chart 7. The evolution of stress field consists in migration of maximum stresses in concordance with mining advance downward. This characteristic complies with the available data on seismic activity and locations of seismic foci [19].

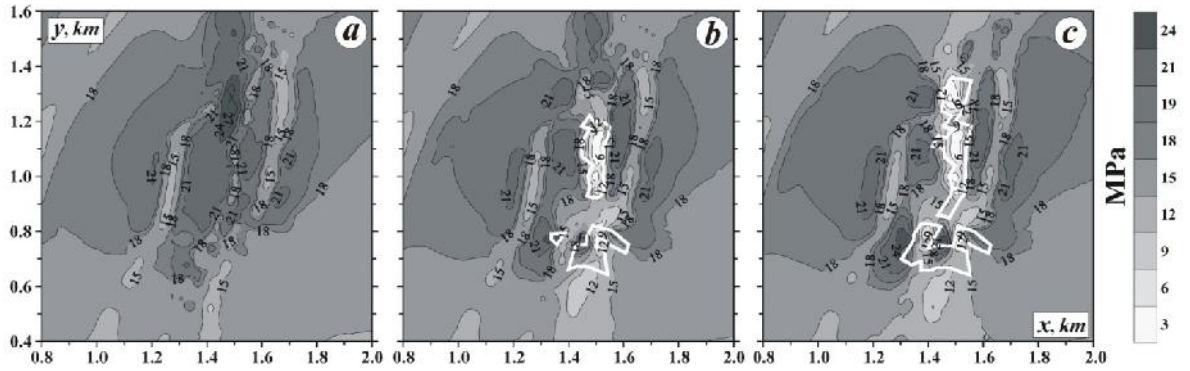

Chart 7. Distribution of maximal shear stress ²$_{max}$ in horizontal cross-section (Level JNQM m) of domain under investigation in different times of mining: a – 1978; b – 1989; c -2009. White lines show outline of worked-out area.

3.2. Joint analysis of parameters of stress state and induced seismicity

The Tashtagol mine seismic events catalogue (about 18000 events in a period from 1989 to 2012, class *C* of energy 1-9) was at our disposal. The data analysis and visualization of seismic event hypocenters showed that with mined-out area increase, the number of events and their total energy tend to grow: the dynamic event hypocenters grasp an ever-extending area. The annual amount of events in the mine raises at the predominance of weak seismic events ($C = 1\text{-}3$).

As noted above the qualitative character of the spatio-temporal distribution of the rock pressure dynamic manifestations corresponds to direction of mining expansion at deeper levels and higher ore extraction. Meanwhile the developed geomechanical model provides a means for the quantitative estimation of the stress field response to variable goaf configuration and revelation of the relation between parameters of induced seismicity (number, locations and energy of seismic events) and stress state variation.

To carry out the space-time analysis, the upper part of modeled region was separated into 420 blocks (42 parallelepipeds B_i 400*400*70 m along corresponding coordinate axes *x*, *y* and *z* at each horizontal Level, Chart 8). The vertical block size equals to the mining level height of 70 m. The horizontal size of the blocks were selected with regard to statistical representativeness of seismic data and the goaf size. Using geomechanical model and mining plans 3D stress distribution in 1978, 1989, 1999, and 2009 were simulated (Chart 7). The intermediate values of the stress tensor components were found by linear interpolation with a year interval.

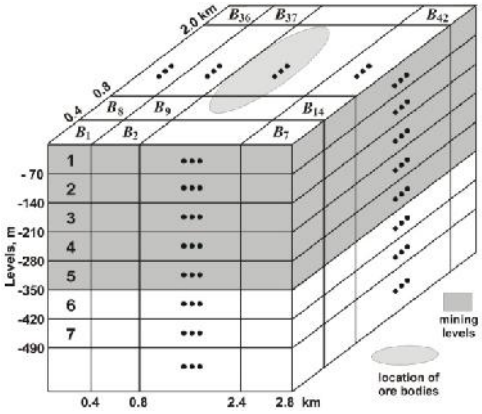

Chart 8. Partition of region under investigation into blocks for statistical analysis of seismic data.

Conventionally dynamic event is associated with failure and most strength criteria "use" the maximum shear stress, thus we considered average value of τ_{max} in block B_i

$$\sigma_i(t_k) = \frac{1}{B_i} \iiint_{B_i} \sigma_{\max}(x, y, z, t_k) dV ,$$

as generalized numerical characteristic of the stress state in time moments t_k=1989, 1990,…,2010 (k = 1,…,22).

Seismic events in available database were classified by energy class C and amount of weak (energy is less than 1 kJ, $C \le 3$) events $N_i(t_k)$ was tallied up for each block B_i. The sampling data for the moderate and strong events (C>3) are non-representative because not more than 2-3 events fall within block B_j annually.

The sample cross-correlation coefficients $\xi_l(i,j)$ were calculated (Tables 1 and 2) in order to reveal the relation between the stress in block B_i and induced seismicity parameters in block B_j at each Level l (Chart 8):

$$\rho_l(i, j) = \frac{\sum (\sigma_i(t_k) - \bar{\sigma}_i)(N_j(t_k) - \bar{N}_j)}{\pm_i(\sigma) \pm_j(N)},$$

where $\pm_i(\sigma) = \sqrt{\sum \left(\sigma_i(t_k) - \bar{\sigma}_i\right)^2}$, $\pm_j(N) = \sqrt{\sum \left(N_j(t_k) - \bar{N}_j\right)^2}$ - the standard deviations; bar denotes average value; summation is carried out over k from 1 to 22; i, j = 1,…42 (Chart 8).

Table 1. Cross-correlation coefficients $\rho_l(i,j)$ for worked-out block B_{25}

Level number	Mining zone		Number of a block in the vicinity of B_{25}								
	25	**18**	**10**	**11**	**12**	**17**	**19**	**24**	**26**	**31**	**32**
1	-0.14	0.28	-	-0.21	-0.05	-0.46	0.17	-0.63	-0.19	-0.43	-0.25
2	–0.55	0.33	-0.42	-0.05	-0.34	-0.54	0.38	-0.54	-0.18	-0.31	-0.40
3	**-0.72**	-0.28	-0.61	-0.61	-0.36	-0.59	-0.08	**-0.83**	-0.68	-0.49	-0.55
4	-0.63	-0.51	-0.23	-0.63	-0.45	**-0.79**	-0.57	**-0.70**	-0.62	-0.51	-0.40
5	-0.51	-0.57	-0.43	-0.50	-0.28	**-0.70**	-0.55	-0.49	-0.50	0.13	-0.38
6	-0.08	-0.22	-0.42	-0.24	-0.21	-0.07	-0.06	-0.40	-0.31	–	-0.28

Table 2. Cross-correlation coefficients $\rho_l(i,j)$ for unmined block B_{17}

Level number	Mining zone		Number of a block in the vicinity of B_{17}								
	25	**18**	**10**	**11**	**12**	**17**	**19**	**24**	**26**	**31**	**32**
1	0.20	-0.20	-0.02	0.27	0.04	0.52	-0.15	0.66	0.23	0.53	0.26
2	0.59	-0.28	0.41	0.16	0.33	0.57	-0.32	0.56	0.24	0.37	0.36
3	**0.70**	0.30	0.58	0.58	0.35	0.64	0.07	**0.80**	0.62	0.44	0.53
4	0.61	0.54	0.28	0.60	0.38	**0.81**	0.57	0.60	0.63	0.45	0.41
5	0.58	0.62	0.45	0.61	0.41	**0.70**	0.67	0.48	0.66	-0.22	0.49
6	0.34	0.49	0.47	0.51	0.44	0.20	0.44	0.41	0.58	-	0.34

Based on $\xi(i,j)$ behavior analysis:

- probably significant relation takes place within the blocks (*inter alia*, values of $\xi_3(25,25)$ and $\xi_3(17,17)$ exceed 0.7);
- these relations weakens with increase of distance from block to zone of mining (for instance, $\xi_1(i,j)$ are low);
- mining of block B_i decreases $\tau_i(t_k)$ while the amount of seismic events raises in the vicinity of B_i, so corresponding correlation coefficients $\xi_l(i,j)<0$ (Table 1);
- at the same time, mining of B_i increases $\tau_i(t_k)$ in the blocks adjacent to B_i because the stress concentrates in surrounding rocks, thus, the number seismic events grows and $\xi_l(i,j)$ are positive (Table 2).

The obtained correlation coefficients are useful to forecast a level of seismic activity in the mine. The blocks B_{17}, B_{24}, B_{25} at Levels 3 and 4 are suitable for this purpose for higher values of $\xi_l(i,j)$ (Tables 1,2).

Using geomechanical model of deposit and the mining production plan up to $t_* = 2018$ (recovery of so called "under-Kondoma" pillar with rich ore located at the Levels –210 and –280 m, see Chart 6*a*) the stress distribution and integral characteristic $\tau_i(t_*)$ were calculated for each block. It is obvious that B_{25} - B_{25} relationship at for Level – 210 m ($\xi_3(25,25) = -0.72$) as well as and B_{17} - B_{25} relationship at the same Level ($\xi_3(17,25)=0.70$) are suitable. It should be noted that stress reduction in B_{25} provokes the growth of seismic event number in B_{25} ($\xi_3(25,25)$ is negative, Table 1) and *vice versa* the stresses increasing in B_{17} leads to increment of the event number in B_{25}.($\xi_3(17,25)$ and $\xi_4(17,25)$ are positive, Table 2).

Having applied the equation of linear regression

$$N_i(t_*) = \P_l(i,j)\frac{\pm_i(N)}{\pm_j(^2)}(^2_j(t_*) - ^2_j) + \overline{N}_i, \qquad (3)$$

for different couples of blocks B_i and B_j, we'll estimate the forthcoming number of seismic events $N_i(t_k)$ with energy class $C \le 3$ in block B_i. Chart 9 demonstrates regression lines (3) for pairs (B_{25}, B_{25}) and (B_{17}, B_{25}) in coordinates (τ,N).

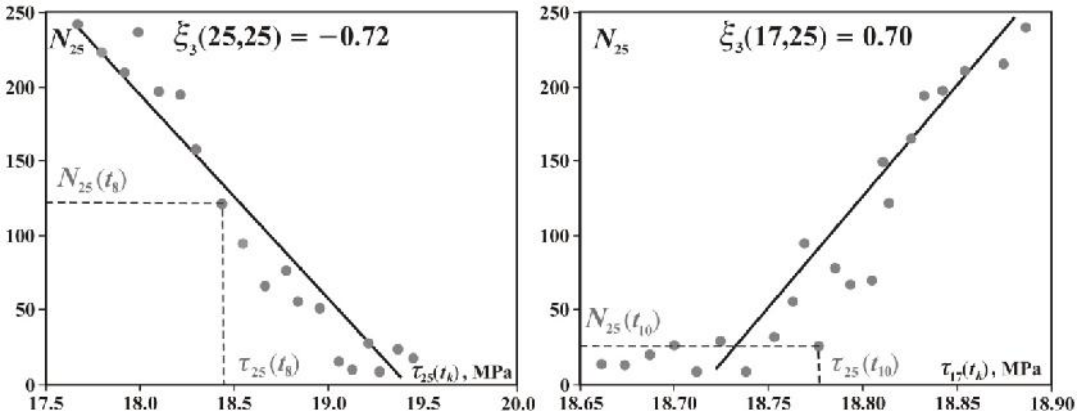

Chart 9. Regression lines for different pairs of blocks that were destined for prediction of seismic events amount.

The prediction results of expected amount $N_{25}(t_6)$ of seismic events (Levels 3, 4) in the course of mining operations are summarizes in the Table 3. It is seen that difference in the obtained numbers appeared no more than 10-15%.

Table 3. Forthcoming amount of seismic events in block B_{25} in 2018 estimated by various pairs of blocks

Numbers in pair of blocks		Level 3 (– 210 m)		Level 4 (– 280 m)	
i	j	$\xi_3(i,j)$	$N_{25}(t_6)$	$\xi_4(i,j)$	$N_{25}(t_6)$
17	25	0.70	**385**	0.61	**275**
25	25	-0.72	**360**	-0.63	**245**

4. CONCLUSION

The method of the joint analysis of stochastic and deterministic information, evaluated using laboratory testing and in situ observation data, allows quantitative relationships between the parameters of geomechanical fields of various physical nature. Based on statistical analysis of induced seismicity (space-and-time distribution

of sources of dynamic events) and variation of stress tensor components in rock mass under mining, the new proposed approach makes it possible to relate the variation in the integral characteristics of stress field and the number and total energy of seismic events in different parts of an object. This enables predictive estimation of induced seismicity parameters at mine planning stage and in actual mining.

5. ACKNOWLEDGMENTS

The work was supported by the Russian Foundation for Basic Research, project no. 15-05-06977.

6. REFERENCE

[1] Urbancic T.I., Trifu C.I.: Recent Advances in Seismic Monitoring Technology at Canadian Mines, J. Appl. Geophysics, 2000, Journal of Applied Geophysics, vol. 45, N 4, pp. 225-237.
[2] Zhenbi L., Baiting Zh.: Microseism Monitoring System for Coal and Gas Outburst, International Journal of Computer Science Issues, 2012, vol. 9, Issue 5, N 1, pp. 1694-0814.
[3] Zakharov V.N.: Seismic-Acoustic Prediction and Monitoring of State and Properties of Rocks in Coal Mining, Moscow: IGD A.A. Skochinskogo, 2002, 172 p. (in Russian)
[4] Kuksenko V.S.: Diagnosis and Forecasting of Failure of Large-Scale Objects, Fizika Tverdogo Tela, 2005, vol. 47, N 5, p.788-792. (in Russian)
[5] McGarr A., Simpson D., Seeber L.: Case Histories of Induced and Triggered Seismicity, International Handbook of Earthquake and Engineering Seismology, 2002, vol. 81A, pp. 647-661.
[6] Mogi K.: Experimental Rock Mechanics, London: Taylor and Francis, 2007, 585 p.
[7] Shkuratnik V.L., Filimonov Yu.L., Kuchurin S.V.: Acoustic-Emissive Memory Effect in Coal Samples under Triaxial Axial-Symmetric Compression, Journal of Mining Science, 2006, Vol. 42, N 3, pp. 203-209.
[8] Vallejous J.A., MacKinnon S.D.: Correlation between Mining and Seismicity for Re-entry Protocol Development, International Journal of Rock Mechanics and Mining Science, 2011, Vol. 48, pp. 616-625.
[9] Al Heib M.: Numerical and Geophysical Tools Applied for the Prediction of Mine Induced Seismicity in French Coal Mines, International Journal of Geosciences, 2012, Vol. 3, N 4A, pp. 834-846.
[10] Larsson L., Sjodahl M., Thuvander F.: 3D Microscopic Displacement Field Measurements Using Digital Speckle Photography, Optics and Lasers in Engineering, 2004, Vol. 4, N 5, pp.767-777.
[11] GOST 21153.2-84. Rocks. Processes for Determination of Ultimate Strength under Uniaxial Tension, Moscow: Gos. Komitet SSSR Stand., 1984. (in Russian)
[12] Jaeger J.C., Cook N.G.W.: Theory and Application of Curved Jacks for Measurement of Stresses, State of Stress in the Earth's Crust, W.R. Judd (Ed.) New York: Elsevier, 1964, pp.381-395.
[13] Gomez J.T., Shukla A., Sharma A.: Static and Dynamic Behavior of Concrete and Granite in Tension with Damage, Theoretical and Applied Fracture Mechanics, 2001, Vol. 36, pp. 37-49.
[14] Oparin V.N. et al.: Zonal Rock Disintegration and the Stability of Underground Workings, Novosibirsk: SO RAN, 2008, 278 p. (in Russian)
[15] Shen B., King A., Guo H.: Displacement, Stress and Seismicity in Roadway Roofs during Mining-Induced Failure, Int. J. of Rock Mech. and Min. Sci., 2008, vol. 45, no 5.
[16] Aki K., Richards P.G.: Quantitative Seismology. Theory and Method, Vol. 1, San Francisco, W.H. Freeman and Company, 1983, 557 p.
[17] Nazarova L.A., Nazarov L.A., and Leont'ev A.V.: Three-Dimensional Geomechanical Model of Tashtagol Iron-Ore Deposit, Journal of Mining Science, 1998, Vol. 34, N 3, pp. 209-216.
[18] Nazarova L.A.: Estimating the Stress and Strain Fields of the Earth's Crust on the Basis of Seismotectonic Data, Journal of Mining Science, 1999, Vol. 35, N 1, pp. 26-35.
[19] Nazarova L.A.: Modeling of Volume Stress Fields in Earth Crust Fault Zones, Doklady Earth Science, 1995, Vol. 342, N 6, pp. 804-808.
[20] Oparin V.N. et al.: Methods and Systems for Seismic-Deformation Monitoring of Induced Earthquakes and Rock Bursts, Novosibirsk: SO RAN, 2009, 304 p. (in Russian)